

# Probabilistic Approach for Road-Users Detection

G. Melotti, W. Lu, D. Zhao, A. Asvadi, N. Gonçalves, C. Premebida

**Abstract**—Object detection in autonomous driving applications implies that the detection and tracking of semantic objects are commonly native to urban driving environments, as pedestrians and vehicles. One of the major challenges in state-of-the-art deep-learning based object detection is false positive which occurrences with overconfident scores. This is highly undesirable in autonomous driving and other critical robotic-perception domains because of safety concerns. This paper proposes an approach to alleviate the problem of overconfident predictions by introducing a novel probabilistic layer to deep object detection networks in testing. The suggested approach avoids the traditional Sigmoid or Softmax prediction layer which often produces overconfident predictions. It is demonstrated that the proposed technique reduces overconfidence in the false positives without degrading the performance on the true positives. The approach is validated on the 2D-KITTI object detection through the YOLOV4 and SECOND (Lidar-based detector). The proposed approach enables interpretable probabilistic predictions without the requirement of re-training the network and therefore is very practical.

**Index Terms**—Object Detection; Overconfident prediction; Probabilistic calibration; Deep learning.

## I. INTRODUCTION

REMARKABLE advances in computing hardware, sensors and machine learning techniques have contributed significantly to artificial perception for autonomous driving [1], [2]. However, even with such progresses, artificial perception in real-world driving still meets grand challenges [1], [3]–[5]. Object detection is a key aspect of perception systems and has been gradually dominated by deep learning (DL) approaches. Generally, modern DL methods export the detection confidence as the normalized scores by the Softmax function (SM) [6] or a single value obtained from the Sigmoid function (SG) [7] without considering the overconfidence or uncertainties in the predictions (see Fig. 1). Such a lack of proper uncertainty prediction and the overconfidence behaviour are undesired, because objects detected as false positives may have high score values without any level of uncertainty. It can be better understood by an example: consider six

Gledson Melotti is with the Federal Institute of Espírito Santo-Brazil, and the ISR-UC at University of Coimbra, Portugal. E-mail: gledson@ifes.edu.br

W. Lu and D. Zhao are with the University of Glasgow and the James Watt School of Engineering, UK. E-mail: {26186051@student.gla, Dezong.Zhao@glasgow}.ac.uk

Alireza Asvadi is with IMT Atlantique, France. E-mail: alireza.asvadi@imt-atlantique.fr

C. Premebida and N. Gonçalves are with the University of Coimbra and the Institute of Systems and Robotics (ISR), Portugal. E-mail: {cpremebida, nunogon}@isr.uc.pt

Manuscript received in 2021.

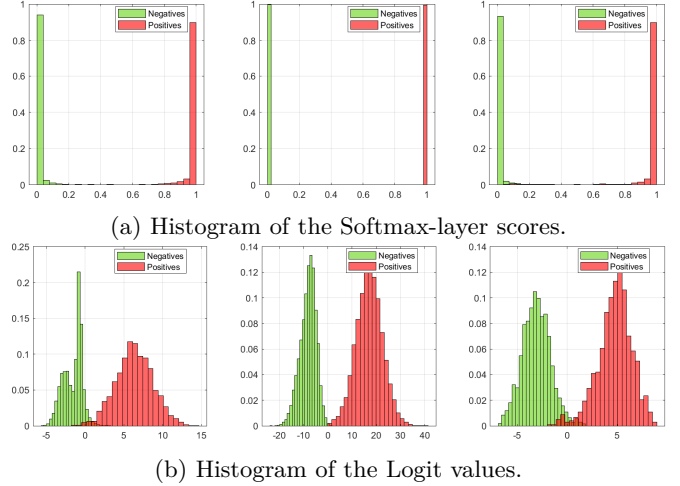


Fig. 1: In (a) we can see the overconfidence problem regarding the predictions using Softmax for a three classes case (from left to right: pedestrian, car and cyclist). The Logits values (*i.e.*, the layer that feeds into Softmax) have been normalized and the corresponding distributions are modelled by a histogram in (b).

deep networks trained to classify three classes of objects namely, car, cyclist, and pedestrian. The detection confidence values for each object have been obtained through a prediction layer, such as the Softmax layer, which then normalizes the values within the interval  $[0, 1]$ . As shown in Table I, the networks show satisfactory results in terms of F-scores [8], [9] on a test set. However, what would happen when an object out of the trained classes is presented to the networks? A clue to answering this question is given by Fig. 2, where an object representing ‘vegetation’ class<sup>1</sup> has been classified with an extremist prediction (*i.e.*, value very close to one, indicating overconfident behaviour) to one of the three trained classes. Ideally, the expected value for that example would be close to 0.3, as the object does not belong to any of the three classes considered in the training. More representative cases of overconfident predictions considering out-of-training distribution examples are shown by histograms in Fig. 3, considering different classes *e.g.*, ‘person-sitting’, ‘tree’, ‘pole’.

The ability to properly represent the uncertainties of predictions of an object detection system would ensure safer decision-making actions, specially in autonomous driving and robotic systems which may pose threat to people’s lives [16]. In the literature, the uncertainties of a deep learning model [17]–[20] can be obtained through the pre-

<sup>1</sup>The vegetation class was not considered on the training set.

TABLE I: Classification results using F-score metric by deep network models.

Model	Car	Cyclist	Pedestrian	Average
LeNet [10]	99.17	89.08	93.79	94.02
AlexNet [11]	99.42	91.41	96.46	95.75
Inception V3 [12]	99.68	95.05	97.67	97.46
EfficientNetB1 [13]	99.84	97.43	98.74	98.67
ViT [14]	99.46	93.56	96.37	96.46
MLP Mixer [15]	98.98	87.47	92.42	92.96

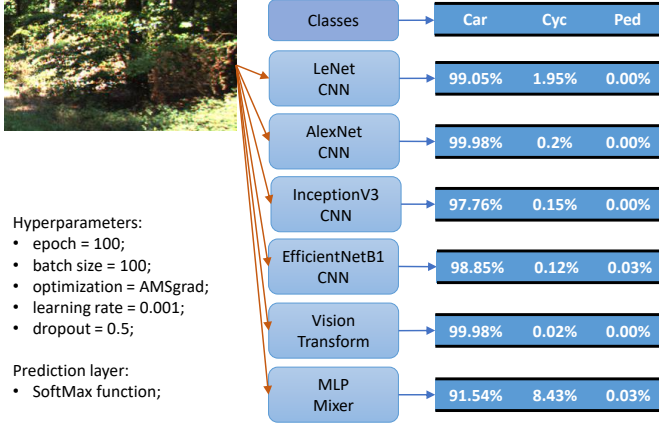


Fig. 2: Example of classifying an out-of-(training)distribution test object. The object has been classified by six different neural networks, and all the models' outputs are overconfidence - which may have critical implications.

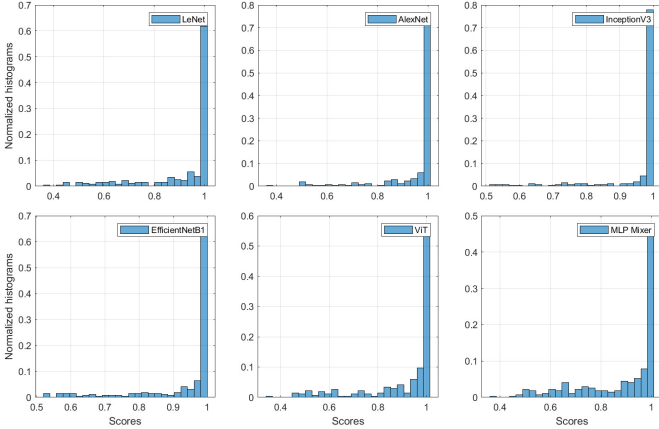


Fig. 3: Object classification on out-of-distribution test dataset through six different neural networks, using Softmax as the prediction layer, considering the LeNet [10], AlexNet [11], InceptionV3 [12], EfficientNetB1 [13], Vision Transformer [14], and MLP Mixer [15] CNNs. The overconfident behavior is notorious.

dicted values (calibration techniques) or via the network weights/loss function (regularization techniques) [21]–[33]. However, we will see that calibration and regularization techniques are not immune to the overconfidence problem as well, as detailed in Section II. An alternative to reduce overconfidence predictions, and in some techniques to

enable probabilistic interpretation, can be attained by looking at the Logit-layer values (*i.e.*, the score-values before the prediction layer, or activation functions) [17]–[20] - as illustrated in Fig. 1b which presents a more tractable distribution than the distribution out of the Softmax prediction layer.

In this context, this paper presents a new methodology to reduce overconfidence predictions in deep object detection networks without interfering in the cost function and/or re-training the network. Furthermore, this paper shows that calibration techniques (such as temperature scaling and Monte Carlo Dropout, as well as confidence penalty, and Bayesian neural networks) may provide overconfidence results. In summary, the contributions are:

- An investigation of the predicted values using distributions from the Logit-layer data;
- An efficient way to obtain proper probabilistic inference via Maximum Likelihood (*ML*) and Maximum a-Posteriori (*MAP*) formulations;
- Detailed comparisons between the *ML/MAP* against the Sigmoid layer, considering true and false positive predictions by YOLOV4 and SECOND, with respect to overconfidence results;
- Comprehensive results showing that the traditional prediction layers can induce erroneous decision-making in deep object detection networks.

## II. RELATED WORK ON OVERCONFIDENCE PREDICTION

Generally, the formulations that acts directly on the predicted scores to reduce overconfidence predictions of learning models are considered as calibration techniques. On the other hand, the formulations that interfere with the weight updates to improve the generalization ability and, eventually, eliminate overconfidence are considered as regularization techniques [27]. Well-calibrated or well-regularized models are expected to provide accurate predictions when they are right about object detection and, conversely, provide high uncertainty when they are inaccurate about a detection. However, such techniques to reduce or mitigate overconfidence are still to be improved [21]. Actually, recent studies have shown overconfidence predictions as unsolved problems in the field of deep learning [21], [34]–[37]. Consequently, several probabilistic methods have been proposed as an alternative to reduce overconfidence predictions, as well as to capture uncertainties in deep neural network models [17]–[20], [22]–[26], [28]–[33], [38]–[41].

The following subsections present in more details about the most common and recent calibration techniques (temperature scaling [27], Monte Carlo Dropout [29], [42]) and regularization techniques (penalization of overconfidence output distributions [24], [26], [28], [39], [41], label smoothing [43]). Additionally, we would discuss the disadvantages of the mentioned techniques when predicting objects belonging to out-of-training-distribution data (which may be critical in autonomous driving and robotics).

### A. Softmax and Sigmoid Prediction Layers

Softmax is currently one of the most commonly employed functions to act as the prediction layer in deep networks. In part, this is explained by the fact that such function increases the weights of the correct classes in an exponential way, strongly interfering in the updating of the weights, and thus may guarantee a better result in terms of classification performance. However, such behaviour may lead to overfitting, since the model becomes overconfident on the training data [44]. Additionally, the Softmax function does not provide any confidence measure for the predicted values, similarly for non-calibrated models [27], [45], [46]. Also, it is possible to find in the literature works where the Softmax's outputs are considered actual probabilistic values (perhaps because they sum up to one) which tends to give an erroneous interpretation about probabilistic results.

The Softmax, as well as the Sigmoid function, is sensitive to adversarial attacks. The studies that back this claim consider adversarial perturbations applied to the Softmax and Sigmoid prediction layer, generating possible underfitting problems on the weights [47], [48]. Additionally to the fact that Softmax and Sigmoid functions are prone to provide poorly calibrated scores and being sensitive to adversarial attacks. Thus, such functions seem to be inadequate to cope with out-of-distribution objects in the test phase for example, during the evaluation time the trained network can be faced with objects that do not fit to any of the training classes, as demonstrated experimentally in [18], [41], [46], [49]–[51].

### B. Calibration

Among the various existing techniques [27], temperature scaling has demonstrated interesting characteristics because it is simple and, in some cases, efficient. Another technique that can be considered as calibration is the Monte Carlo Dropout formulation [42], with the benefit of providing uncertainty about the predictions.

1) *Temperature Scaling*: the value of temperature scaling ( $TS$ ) is obtained by minimizing the negative log likelihood (NLL) on the validation set. All the values of the logit vector (before the prediction layer) are multiplied by a scalar parameter  $\frac{1}{TS}$ , with  $TS > 0$ . Simply, the temperature scaling parameter can be included in the Softmax prediction layer (SM)

$$SM(\hat{z}_j) = \frac{e^{(\hat{z}_j/TS)}}{\sum_{k=1}^K e^{(\hat{z}_k/TS)}}, \quad (1)$$

where  $k \in \{1, \dots, K\}$ ,  $K$  is the number of classes,  $\hat{z}_j$  is the output of the predicted logit layer *i.e.*, predict score value of the object  $j$ .

2) *Monte Carlo Dropout*: dropout [29], [42] is a stochastic technique [51], which might potentially be included in the neural network, contributing to avoid overfitting. It is usually used during training, and therefore it can

be questioned: what does occur when the dropout is used during testing? The predicted values will not be deterministic *i.e.*, the values depend on which connections between the neurons will be randomly chosen during the prediction stage. In fact, the same test sample forwarded several times in the network can have different predicted values.

### C. Regularization

Different from the calibration techniques, regularization acts, during the training process, on the updates of the weights according to the cost function [12], [28], [43]. Nevertheless, regularization techniques do not provide any measure of uncertainty about the predictions. On the other hand, the Bayesian neural networks' formulations - which can be considered a regularization technique as well - indeed capture the model's uncertainties [40], [41], [52].

1) *Confidence Penalty and Label Smoothing*: for classification problems, defining  $\mathbf{X} = \{\mathbf{x}_1, \dots, \mathbf{x}_j\}$  as input data, and  $\mathbf{Y} = \{\mathbf{y}_1, \dots, \mathbf{y}_j\}$  as output data obtains the dataset  $D = \{\mathbf{x}_j, \mathbf{y}_j\}_{j=1}^{N_{ts}}$ , where  $N_{ts}$  is training set size,  $\mathbf{x}_j \in R^n$ , and  $\mathbf{y}_j \in \{1, \dots, K\}$  with  $K$  classes, the loss function considering the true label as one-hot encoding vector is defined by

$$\mathcal{L} = -\frac{1}{N_{ts}} \sum_j^{N_{ts}} p(\mathbf{y}_j|\mathbf{x}_j) \log(p(\hat{\mathbf{y}}_j|\mathbf{x}_j)), \quad (2)$$

where  $p(\mathbf{y}_j|\mathbf{x}_j)$  is the distribution of the true label (ground-truth) given the data,  $\hat{\mathbf{y}}_j$  is the predicted value for the input  $\mathbf{x}_j$ , and  $p(\hat{\mathbf{y}}_j|\mathbf{x}_j)$  is the predicted labels distribution.

The expression of the confidence penalty (3) includes a weighting term in the cost function given in (2). The additional term is the Entropy of the predicted values, and  $\beta$  is the parameter that controls the confidence penalty [28]

$$\mathcal{L} = -\frac{1}{N_{ts}} \sum_j^{N_{ts}} [p(\mathbf{y}_j|\mathbf{x}_j) \log(p(\hat{\mathbf{y}}_j|\mathbf{x}_j)) - \beta p(\hat{\mathbf{y}}_j|\mathbf{x}_j) \log(p(\hat{\mathbf{y}}_j|\mathbf{x}_j))]. \quad (3)$$

Unlike confidence penalty, the label smoothing technique does not directly interfere with the cost function. In fact, label smoothing modifies the extreme values of the one-hot encoding vector, as defined in (4) [12]

$$\mathbf{y}_{\text{new},j,k} = (1 - \epsilon)\mathbf{y}_{j,k} + \frac{\epsilon}{K}, \quad (4)$$

where  $\mathbf{y}_{j,k}$  is the object  $j$  in the class  $k$ ,  $\mathbf{y}_{\text{new},j,k}$  is the new label value,  $\epsilon$  is the smoothing parameter, and  $K$  is the number of classes.

2) *Bayesian Neural Network*: a network that is modelled using Bayes' inference (5) to assign probabilities to events, and thus capturing uncertainties in a model's predictions, by considering the network weights as a probability distribution parameter(s) instead of a 'deterministic' number. The posterior probability of the weights given the

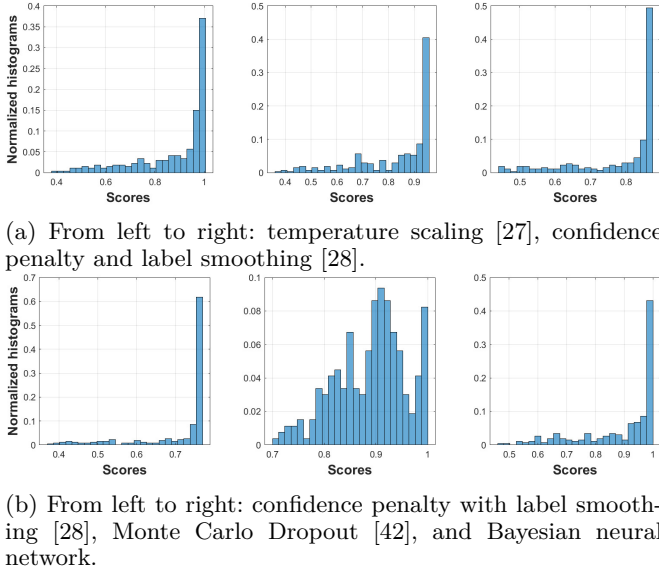


Fig. 4: Object classification on out-of-(training)-distribution test dataset using calibration and regularization techniques in an InceptionV3 CNN model.

input and the target/class data can be expressed by [29], [40]

$$p(\mathbf{W}|\mathbf{X}, \mathbf{Y}) = \frac{p(\mathbf{Y}|\mathbf{X}, \mathbf{W})p(\mathbf{W})}{p(\mathbf{Y}|\mathbf{X})}, \quad (5)$$

where  $\mathbf{W} = \{\mathbf{w}_1, \dots, \mathbf{w}_i\}$  denotes the weights matrix,  $\mathbf{X}$  is input data,  $\mathbf{Y}$  is output data,  $p(\mathbf{W})$  is the prior distribution, which expresses the uncertainty before any data observed [52], [53], and  $p(\mathbf{Y}|\mathbf{X}, \mathbf{W})$  is the class conditional density (likelihood function). The  $p(\mathbf{Y}|\mathbf{X}) \neq 0$  acts as a scaling factor for  $p(\mathbf{W}|\mathbf{X}, \mathbf{Y})$ , and it can be expressed as  $\int p(\mathbf{Y}|\mathbf{X}, \mathbf{W})p(\mathbf{W})d\mathbf{W}$  that can often be determined by the law of the total probability [52]. For example, considering a discrete case<sup>2</sup>,  $P(\mathbf{Y}|\mathbf{X})$  can be computed per parameter  $\mathbf{w}_i$  *i.e.*,  $\sum P(\mathbf{Y}|\mathbf{X}, \mathbf{w}_i)P(\mathbf{w}_i)$ .

The calculation of the posterior  $p(\mathbf{W}|\mathbf{X}, \mathbf{Y})$  may not be trivial because the density function  $p(\mathbf{Y}|\mathbf{X})$  can assume a complex form, whereas the prior can be specified from some previous knowledge and the likelihood conceivably obtained from the data.

As mentioned above, posterior distribution may not have an analytical solution [52]. Thus, a possible solution is to perform an approximation by means of variational inference [30]–[32], [39], [42], [52]–[54].

#### D. Discussion on the State of the Art

Temperature scaling, confidence penalty, and label smoothing techniques aim to reduce the overconfidence problem when making predictions using relatively simple

formulations and with the advantage of no need to re-train the network. The disadvantage of these techniques is the inability to directly provide an uncertainty interval regarding the detected objects subjected to the trained classes. Monte Carlo Dropout and Bayesian neural networks, on the other hand, provide uncertainties measures *i.e.*, the mean and variance, but the computational cost is high.

Figure 4 shows the performance of some calibration and regularization techniques by considering out-of-distribution test objects (‘person sitting’, ‘tree’, ‘pole/stem’). The networks were trained from scratch to classify objects belonging to the categories {‘car’, ‘cyclist’, ‘pedestrian’}, considering  $\epsilon = 0.2$  in (4) for label smoothing,  $\beta = 0.3$  in (3) for the confidence penalty,  $TS = 1.82$  in (1) for temperature scaling, and for Monte Carlo Dropout the test sample was forwarded 300 times through the network. In the case of the Bayesian neural network, the classification experiments were conducted using the Tensorflow toolbox. Note that most of the objects in this controlled experiment have been classified with overconfidence.

The overconfidence problem in deep-models can be detrimental to draw a firm conclusion regarding safety, particularly because it is not possible to foresee all kinds of objects that can appear, for example, within a perception system’s FOV of an autonomous vehicle operating in a real-world (uncontrolled) environment. However, it can be partially concluded that the behavior shown in Fig. 4 makes it very difficult to interpret the model’s confidence in a proper way.

### III. PROBABILISTIC INFERENCE FOR OBJECT DETECTION

This section presents a formulation to reduce overconfidence predictions on existing deep object-detectors, including non-parametric and parametric modeling to represent the likelihood and the priors. The proposed approach relies on a Maximum Likelihood (ML) and Maximum a-Posteriori (MAP) function-layers, based on the Bayes’ rule, to replace Softmax or Sigmoid functions depending on the object detector.

#### A. ML and MAP Layers

The formulation behind the Bayesian inference for the proposed ML and MAP layers is built up from the Logit outputs/scores (denoted by  $\mathbf{x}$ ) and the random variables  $\mathbf{C}$  and  $\mathbf{W}$  *i.e.*, the class-labels and the network weight respectively. The decision layers will then output a posterior  $P(\mathbf{C}|\mathbf{x}, \mathbf{W})$  that is proportional to the class-conditional density (*i.e.*, likelihood)  $p(\mathbf{x}|\mathbf{C}, \mathbf{W})$  and the priors  $P(\mathbf{C})$ , where  $\mathbf{C} = \{c_1, \dots, c_N\}$  and  $\mathbf{x} = \{x_1, \dots, x_N\}$ , with  $x_i$  corresponding to the Logit value for the class  $c_i$ . Thus, the Bayes’ rule may simply be given by (6), considering that the weights were the result of a learning process in order to explain the data [53] and are assumed to be constant after the training,

$$P(\mathbf{C}|\mathbf{x}) = \frac{p(\mathbf{x}|\mathbf{C})P(\mathbf{C})}{p(\mathbf{x})}. \quad (6)$$

<sup>2</sup>Probability formulations for continuous cases are represented by lowercase letters, while for discrete cases they are represented by uppercase letters.

The law of total probability [52], [55] allows (6) to be rewritten using the *per-class* discrete formulation,

$$P(c_i|\mathbf{x}) = \frac{P(\mathbf{x}|c_i)P(c_i)}{\sum_{i=1}^K P(\mathbf{x}|c_i)P(c_i)}, \quad (7)$$

where  $K$  is the number of classes.

Inference can then be made on the test set regarding  $\mathbf{C}$  given the dependence with  $\mathbf{x}$  *i.e.*, the value of the posterior probability (7) of  $\mathbf{C}$  is determined after observing the value of  $\mathbf{x}$ . Once we have specified the likelihood distribution  $p(\mathbf{x}|\mathbf{C})$ , and the priors, the proposed ML/MAP prediction layers can be used to replace a Softmax or a Sigmoid function in order to output the object classification scores in a probabilistic way. Thus, the Maximum Likelihood (*ML*) and Maximum a-Posteriori (*MAP*) functions can be defined as prediction layers at the testing time, and they are expressed by

$$ML = \arg \max_i \frac{(P(\mathbf{x}|c_i) + \lambda)}{\sum_{i=1}^K (P(\mathbf{x}|c_i) + \lambda)}, \quad (8)$$

$$MAP = \arg \max_i \frac{(P(\mathbf{x}|c_i)P(c_i) + \lambda)}{\sum_{i=1}^K (P(\mathbf{x}|c_i)P(c_i) + \lambda)}, \quad (9)$$

where  $\lambda$  is an additive smoothing parameter to avoid the “zero” probability issue [56]–[58], to indirectly mitigate the overconfidence problem, and at the same time incorporate some unpredictable level of uncertainty in the final prediction (mainly motivated by out-of-distribution objects). The parameter  $\lambda$  is not too high or too small, and does not depend on any specific prior information, but its value has to preserve the original distribution ‘shape’ without degrading the final result.

Notice that, although the Bayesian formulation takes distributions into account, *ML* and *MAP* layers compute a single estimate rather than a distribution.

### B. Estimating the Likelihood and Prior Probability

The non-parametric probabilistic density distribution chosen here to obtain the likelihood function comes from normalized histograms<sup>3</sup> of the Logit-layer’s scores for each class on the training dataset, as shown in Fig. 5.

During the testing phase (*i.e.*, on the test set), the Logit-layer score per example (or object) will then be matched to the per-class histogram, as illustrated in Fig. 6.

Unlike the likelihood function estimation, the prior probability distribution has been modelled by a Normal. Thus, the parametric estimation depends on the mean and the variance obtained from the Logit scores as well (this time it is a continuous pdf as shown in Fig. 7). Therefore, the prior is  $P(c_i) \sim \mathcal{N}(\mathbf{x}|\mu, \sigma^2)$  with mean  $\mu$  and variance  $\sigma^2$  computed per class.

<sup>3</sup>The importance of normalizing the histogram is to ensure that the sum of the probabilities is one.

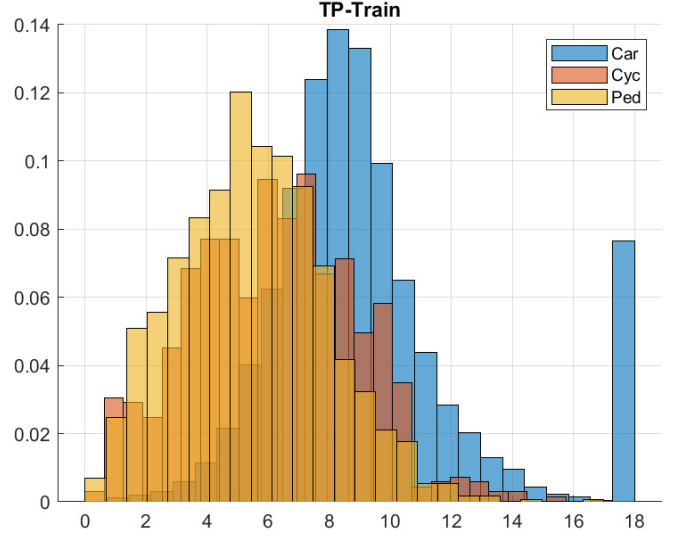


Fig. 5: Logit layer output *i.e.*, before the prediction layer.

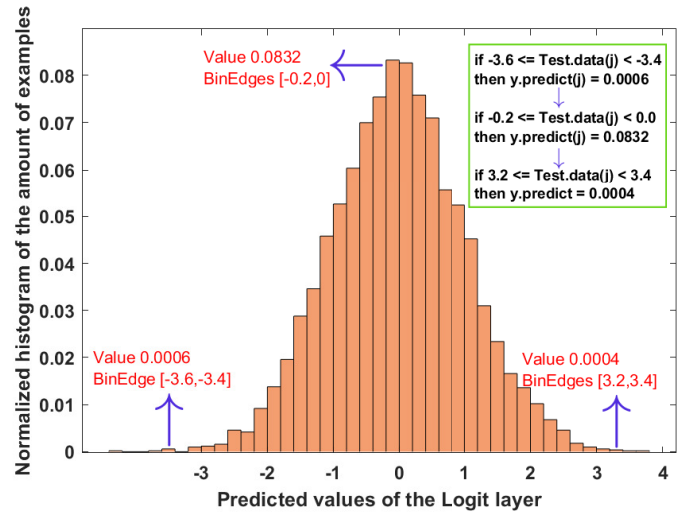


Fig. 6: Obtaining probability values out of a histogram generated using the Logits on the training set.

Algorithm 1 summarizes the steps to calculate the scores in the *ML* and *MAP* layers. Note that detection models generally consider the confidence level of the detected object [7] *i.e.*, the product of the objectness (objectiveness) and the class scores. Likewise, the proposed methodology considers the class score to compute *ML* and *MAP* layer values, and then the values obtained from the *ML* and *MAP* layers are multiplied by the objectness scores obtained directly from the detection model.

The purpose of considering a discrete (histogram) and a continuous pdf to model the likelihood and the *a-prior* probability respectively, is motivated from the perspective of complementary information that can be extracted from the same data.

## IV. OBJECT DETECTION

Currently, the state of the art in pattern recognition for autonomous driving and robotics is closely related to



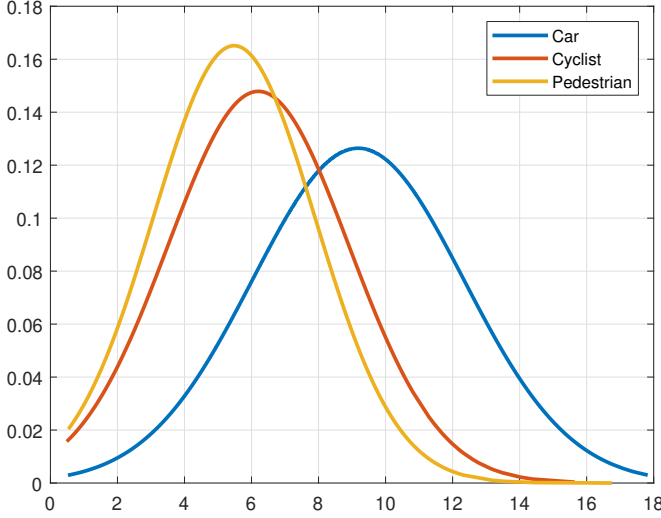


Fig. 7: Gaussian distributions to estimate the prior probabilities for the three training classes (car, cyclist and pedestrian).

#### Algorithm 1: *ML* and *MAP* Layers

##### Input:

- Densities (normalized histogram and Gaussian distribution on the training set, Fig. 6);
- Logit-layer values on the test set ( $test_{Lg}$ );
- Additive smoothing ( $\lambda$ );
- Number of classes ( $K$ ).

##### Output:

- Maximum Likelihood (*ML*);
- Maximum a-Posteriori (*MAP*).

##### Getting the likelihood:

$P(\mathbf{x}|\mathbf{C}) \leftarrow \text{zeros}(\text{size}(test_{Lg}), K);$

```

for  $t \leftarrow 1 : \text{size}(test_{Lg})$  do
  for  $j \leftarrow 1 : K$  do
    for  $i \leftarrow 1 : \text{size}(\text{BinValues}(j))$  do
       $P(\mathbf{x}|c_i)(t, j) \leftarrow \text{BinValues}(j);$ 
    end
  end
end

```

##### Getting the Prior:

$P(\mathbf{C}) \leftarrow \mathcal{N}(test_{Lg} | [\mu_{train}, \sigma_{train}^2]);$

##### Calculating the *ML* and *MAP*:

```

 $\lambda \leftarrow 0.01;$ 
 $ML \leftarrow P(\mathbf{x}|\mathbf{C}) + \lambda;$ 
 $ML \leftarrow (ML / \text{sum}(ML)) * \text{ObjectnessScore};$ 
 $MAP \leftarrow P(\mathbf{x}|\mathbf{C})P(\mathbf{C}) + \lambda;$ 
 $MAP \leftarrow (MAP / \text{sum}(MAP)) * \text{ObjectnessScore};$ 

```

object detection using deep models, which has become one of the most important areas of computer vision (including LiDAR-based systems). The primary purpose of a detector is to estimate the object’s position, size and class/category. A 2D detector estimates bounding boxes considering the

coordinates of the center, width and height of the objects’ hypothesis. Additionally, detectors estimate the classification score *i.e.*, predicted class, and an objectness score (confidence threshold). In plain words, the recent detectors rely on a series of steps to define the bounding boxes and the classification scores depending on comparisons across thresholds between predicted output and ground-truth (training stage), as well as objectness score threshold ( $\tau_{obj}$ ), intersection over union (IoU), non-max suppression (NMS), and class threshold.

Among the various detection models, we have chosen the YOLOV4 [7], published in 2020, which at the time has reached the state of the art performance on the COCO dataset, while achieving shot inference time. The structure of YOLOV4 and the proposed methodology is illustrated in Fig. 8.

The advantages of YOLOV4, over previous versions and other existing object detection algorithms, are that YOLOV4 tries to avoid overconfidence results by using data augmentation (CutMix and Mosaic), class label smoothing, and dropout in the convolution layers (Drop-Block regularization), which then influence the classifier accuracy. Also, unlike many object detection algorithms, YOLOV4 uses the Mish activation function instead of the traditional functions (*e.g.*, ReLU, ELU, SeLU, PreLU, Swich). Additionally, YOLOV4 incorporates the Complete IoU cost function [59], as well as cosine annealing scheduler (learning rate) [60], a modified cross-iteration batch normalization [61], self-adversarial training [7]. Finally, the Sigmoid function is employed to get the final bounding boxes and the respective classification scores.

Even though YOLOV4 considers strategies to reduce overconfidence predictions, our results demonstrate that a significant number of false positives are predicted with high score values, which demonstrates that the prediction layer using the Sigmoid function did not mitigate overconfident results enough, as shown in Fig. 9.

For object detection with 3D point clouds, we choose the lightweight yet effective SECOND [62] detector as the baseline. SECOND extracts features by encoding voxel-based 3D data with submanifold sparse 3D convolution layers [62]. The 3D features are converted to Bird’s Eye View (BEV) representations via high compression, where the height in the metric space is flattened into the feature channels. Standard 2D convolutions are used to generate BEV features. The outputting feature map is passed to the single-stage anchor-based detector head for classification and bounding box regression. Compared to the sophisticated models with more structure information, the voxel-based SECOND [62] has a much faster runtime with comparable performance.

As shown in Fig. 10, SECOND [62] outputs a similar distribution, in a *lato sensu* perspective, of the true positives as YOLOV4, while giving distinct and more “aggressive” decisions on the false positives.

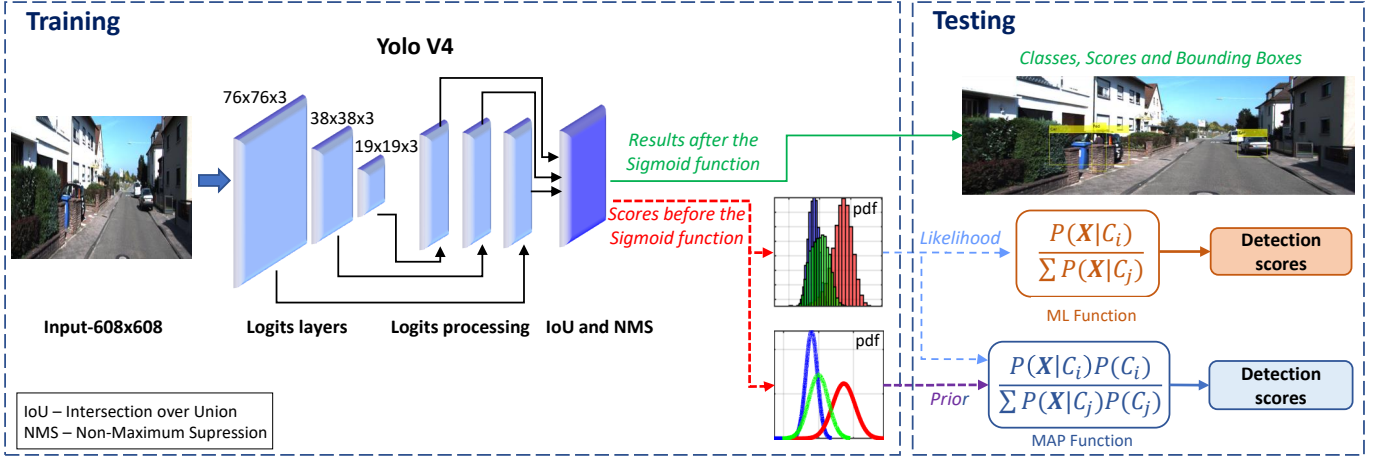


Fig. 8: YOLOV4 representation with Logits and Sigmoid (SG) layers, Maximum Likelihood (ML) and Maximum a Posterior (MAP) functions. After training, the predicted values from the Sigmoid Layer were replaced by the scores from ML and MAP functions. Notice that the YOLOV4 was not trained or re-trained with the ML/MAP functions.

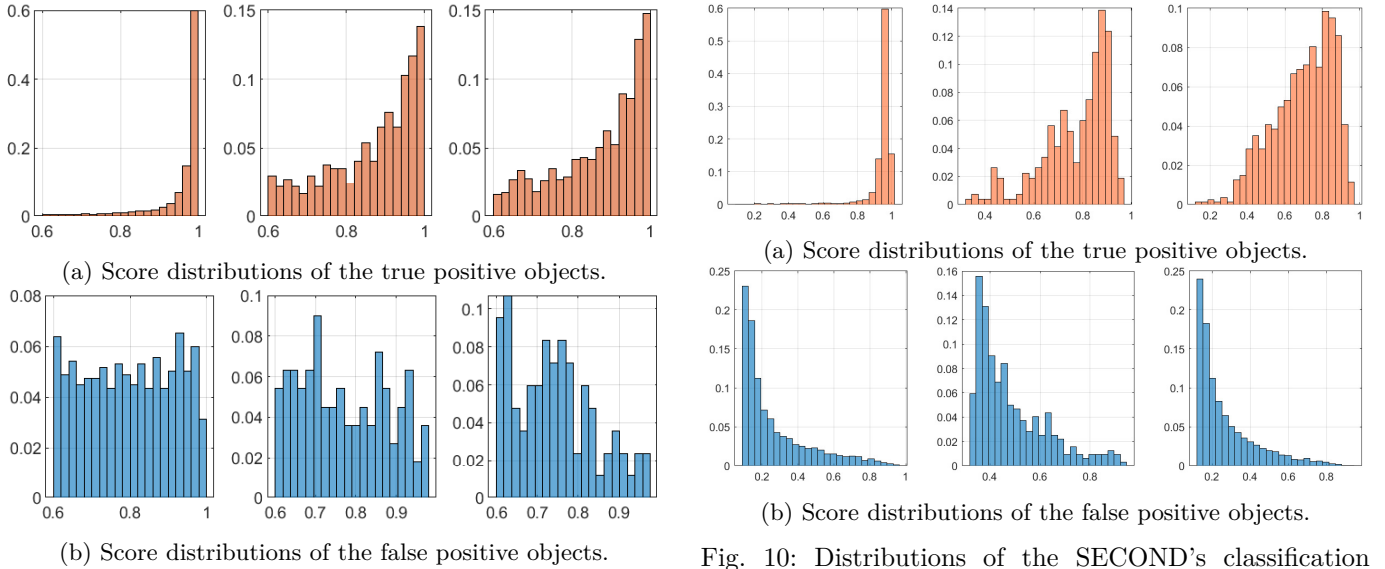


Fig. 9: Distributions of the YOLOV4's classification scores for car, cyclist, and pedestrian classes, considering RGB modality.

#### A. RGB and LiDAR Modalities

The proposed probabilistic methodology is validated through multi-sensory 2D and 3D object detection on the KITTI dataset, considering for YOLOV4 detector RGB images, range-view (RaV), and reflectance-view (ReV) maps modalities, as showed in Fig. 11, and 3D point clouds for SECOND detector. The modalities (RaV), and (ReV) were obtained by projecting the 3D-LiDAR point clouds in the 2D image plane followed by an upsampling step using a tailored bilateral filter implementation, expressed in (10), where  $\hat{r}_0$  is the upsampled pixel [63]

$$\hat{r}_0 = \frac{1}{W} \sum_{i=1}^n G_{\sigma_s}(\|c_0 - c_i\|) G_{\sigma_r}(|r_0 - r_i|) r_i, \quad (10)$$

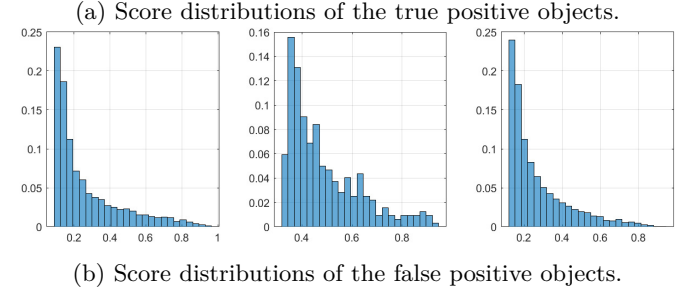


Fig. 10: Distributions of the SECOND's classification scores for car, cyclist, and pedestrian classes, considering LiDAR modality (3D LiDAR).

where  $W = \sum_{i=1}^n G_{\sigma_s}(\|c_0 - c_i\|) G_{\sigma_r}(|r_0 - r_i|)$  is a scaling factor that ensures the output sums to one,  $G_{\sigma_s}$  weights the point  $c_i$  inversely proportional to a distance (we used the Euclidean distance), and  $G_{\sigma_r}$  weights the sampled points from their intensity values  $r_i$ .  $G_{\sigma_s}$  and  $G_{\sigma_r}$  were considered to be of the form

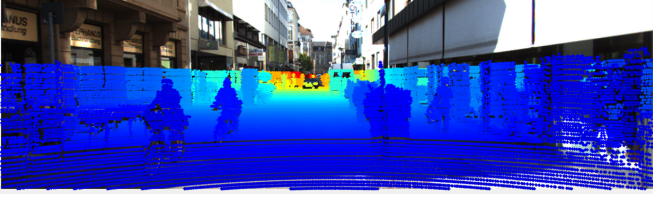
$$G_{\sigma_s} = \frac{1}{1 + (\|c_0 - c_i\|)}, \quad (11)$$

$$G_{\sigma_r} = \frac{1}{1 + (|r_0 - r_i|)}. \quad (12)$$

In fact, the upsample is for estimating points at positions where there are no projected points. The estimate of such points can be performed by considering a mask  $C_{mask}$  of size  $c \times c$  pixels, and using the sliding window

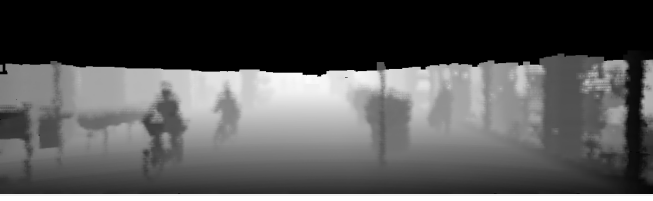


(a) RGB modality.



(b) Projection of the 3D point clouds in the 2D image plain.

Fig. 11: The 3D cloud points were obtained from the Velodyne 64 sensor and then projected onto the image plane.



(a) RaV map generated from LiDAR's depth data.



(b) ReV map using the LiDAR's reflectance data.

Fig. 12: Maps generated by bilateral filtering using sliding window with size  $13 \times 13$ .

principle. The sampled point  $\hat{r}_0$ , located at the center of  $C_{mask}$ , is weighted by the number of neighboring points defined by the mask size *i.e.*, the formulation combines the intensity and distance values of a pixels group which are inside the mask  $C_{mask}$ , being  $c_0 = (c_h, c_v)$  the  $M$  center, which is the localization of interest, and  $\hat{r}_0$  the value to be estimated at  $c_0$  from the  $r_i$  (RaV or ReV), where  $c_h$  and  $c_v$  are the positions in the horizontal and vertical directions respectively, as in Fig. 12.

## V. EXPERIMENTS AND RESULTS

In this section, we evaluate quantitatively the proposed approach to reduce overconfidence predictions through the  $ML$  and  $MAP$  layers, considering Gaussian distributions, and normalized histograms, to model the prior and likelihood respectively. The approach depends of some “hyperparameters” that interfere in the results achieved

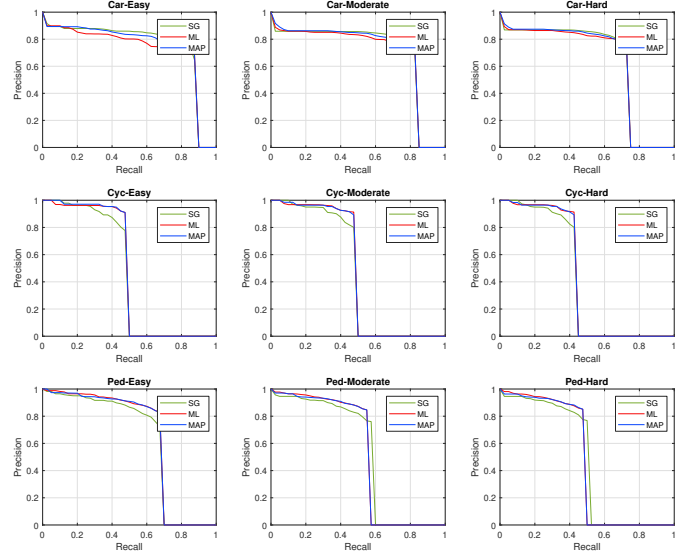


Fig. 13: Precision-recall curves for car, cyc. and ped. classes using the RGB modality, with  $\lambda_{ML} = 5 \times 10^{-3}$ ,  $Bins_{ML} = 22$ ,  $\lambda_{MAP} = 1 \times 10^{-4}$ , and  $Bins_{MAP} = 24$ .

by the  $ML$  and  $MAP$  layers. The additive smoothing  $\lambda$  (c.f. Sect. III-A), the chosen densities *e.g.*, the numbers of bins of the normalized histograms (described in Sect. III-B above), are design dependent parameters and hence are subjected to the problem in hands. Here, the choice of these parameters has been made experimentally.

The experiments conducted in this Section to assess the proposed technique and to support comparison studies make use of the KITTI ‘Object Detection’ dataset<sup>4</sup>, both the RGB (camera) and the LiDAR modalities (necessary for the RaV, ReV, and 3D point cloud). We have split the original training set by considering 3367 frames for training, 375 for validation, and then the remaining 3739 frames comprise the actual test set. RGB, RaV, and ReV modalities were trained with the same hyperparameters (learning rate, image size, anchors, strides, IoU threshold, etc.) for YOLOV4, while the 3D point clouds were trained directly via the SECOND detector.

The results on the *per-modalities* test sets are shown in Figures 13, 14, and 15 through precision-recall curves (Pr-Rc) for YOLOV4, while the Figures 16, 17, and 18 correspond to the experimental results achieved with the SECOND detector. Note that the curves are presented to the three different difficulty levels (easy, moderate and hard), according to the KITTI dataset methodology for object detection. Furthermore, as supplementary material, the scores of the detected objects are shown in Figures 19, 20, 21, and 22 in the Appendix.

In addition to the results given by the Pr-Rc curves, we further present a quantitative comparison, between the baseline (designated by Sigmoid, or simply  $SG$ ) and the proposed  $ML$ , and  $MAP$  layers, using the areas under the curve (AUC), as shown in tables II and III.

<sup>4</sup>[http://www.cvlibs.net/datasets/kitti/eval\\_3dobject.php](http://www.cvlibs.net/datasets/kitti/eval_3dobject.php)



TABLE II: AUC, in %, for the baseline method denoted by *SG*, and the proposed approaches (*ML* and *MAP* layers). The results refer to the **true positives** and have been achieved by the YOLOV4 implementation using 2D representations.

RGB Modality											
Easy				Moderate				Hard			
Case	<i>SG</i>	<i>ML</i>	<i>MAP</i>	Case	<i>SG</i>	<i>ML</i>	<i>MAP</i>	Case	<i>SG</i>	<i>ML</i>	<i>MAP</i>
Car	<b>75.48</b>	71.50	74.15	Car	<b>70.67</b>	69.50	70.54	Car	63.04	62.40	<b>63.11</b>
Cyc	45.47	46.83	<b>47.20</b>	Cyc	45.47	<b>46.78</b>	46.76	Cyc	40.94	<b>42.02</b>	41.99
Ped	61.84	<b>64.10</b>	63.87	Ped	<b>52.27</b>	52.26	52.05	Ped	<b>45.65</b>	45.35	45.10

RaV Modality											
Easy				Moderate				Hard			
Case	<i>SG</i>	<i>ML</i>	<i>MAP</i>	Case	<i>SG</i>	<i>ML</i>	<i>MAP</i>	Case	<i>SG</i>	<i>ML</i>	<i>MAP</i>
Car	<b>82.99</b>	82.31	78.88	Car	71.07	<b>71.49</b>	69.43	Car	62.97	<b>63.31</b>	59.92
Cyc	40.48	<b>44.75</b>	41.61	Cyc	32.28	<b>32.63</b>	31.79	Cyc	28.13	<b>30.25</b>	29.35
Ped	66.27	<b>66.60</b>	63.92	Ped	<b>52.56</b>	52.20	52.00	Ped	<b>45.57</b>	44.96	44.78

ReV Modality											
Easy				Moderate				Hard			
Case	<i>SG</i>	<i>ML</i>	<i>MAP</i>	Case	<i>SG</i>	<i>ML</i>	<i>MAP</i>	Case	<i>SG</i>	<i>ML</i>	<i>MAP</i>
Car	74.42	<b>75.22</b>	74.45	Car	<b>58.13</b>	57.18	56.35	Car	50.83	<b>51.44</b>	50.74
Cyc	30.80	31.32	<b>31.45</b>	Cyc	24.65	26.85	<b>26.95</b>	Cyc	22.73	24.48	<b>24.59</b>
Ped	43.51	43.83	<b>44.08</b>	Ped	33.62	35.23	<b>35.33</b>	Ped	29.32	30.64	<b>30.82</b>

TABLE III: AUC for the *SG*, *ML* and *MAP* layers, using the SECOND detector, considering the true-positive objects.

2D Detection											
Easy				Moderate				Hard			
Case	<i>SG</i>	<i>ML</i>	<i>MAP</i>	Case	<i>SG</i>	<i>ML</i>	<i>MAP</i>	Case	<i>SG</i>	<i>ML</i>	<i>MAP</i>
Car	<b>96.88</b>	93.09	96.57	Car	<b>95.42</b>	93.61	95.24	Car	<b>93.02</b>	91.89	92.88
Cyc	<b>92.66</b>	91.91	92.44	Cyc	<b>80.27</b>	79.65	80.14	Cyc	<b>76.65</b>	76.11	76.52
Ped	70.77	67.22	<b>70.87</b>	Ped	67.74	65.35	<b>67.78</b>	Ped	64.09	62.36	<b>64.16</b>

3D Detection											
Easy				Moderate				Hard			
Case	<i>SG</i>	<i>ML</i>	<i>MAP</i>	Case	<i>SG</i>	<i>ML</i>	<i>MAP</i>	Case	<i>SG</i>	<i>ML</i>	<i>MAP</i>
Car	<b>91.80</b>	79.40	87.27	Car	<b>82.86</b>	75.57	80.32	Car	<b>79.86</b>	75.16	78.15
Cyc	<b>84.21</b>	81.89	82.88	Cyc	<b>67.99</b>	66.59	67.31	Cyc	<b>64.03</b>	62.80	63.50
Ped	<b>57.19</b>	51.45	57.11	Ped	52.39	48.60	<b>52.41</b>	Ped	<b>47.42</b>	44.43	47.38

BEV Detection											
Easy				Moderate				Hard			
Case	<i>SG</i>	<i>ML</i>	<i>MAP</i>	Case	<i>SG</i>	<i>ML</i>	<i>MAP</i>	Case	<i>SG</i>	<i>ML</i>	<i>MAP</i>
Car	<b>93.67</b>	86.44	91.55	Car	<b>89.81</b>	85.64	88.49	Car	<b>88.90</b>	86.24	88.02
Cyc	<b>89.30</b>	87.24	88.59	Cyc	<b>72.41</b>	71.17	72.04	Cyc	<b>68.14</b>	67.07	67.85
Ped	61.98	57.26	<b>62.07</b>	Ped	57.82	54.83	<b>57.89</b>	Ped	53.39	51.11	<b>53.41</b>

Based on the Pr-Rc curves using YOLOV4, it is possible to observe that the proposed probabilistic inference (*ML*, and *MAP* layers) outperformed the baseline (*SG* layer) in almost all modalities and for most of the difficulty levels, particularly for the cyclist class, which has the smallest amount of objects in both training and test sets. To facilitate the comparison analysis, Table II contains the AUC from these experiments, where the best achieved detection performances are highlighted in bold. The AUC ‘metrics’ show that the *ML* and *MAP* perform better than the baseline for moderate and hard levels also, we can see that the performance on the easy level tend to be very close to the baseline which is a positive aspect of the techniques.

The SECOND detector receives 3D point-clouds as input thus, besides 3D detection, we have converted the 3D representation to 2D and Bird’s Eye View (*BEV*) for completeness of the results and benchmarking analysis. At first glance, the *ML*, and *MAP* approaches when applied to SECOND demonstrate to be less effective in improving the detection performance. This is due to the amount of

high-scoring (*i.e.*, highly confident) false positives is small in SECOND, as can be analyzed in figures 22 (Appendix A) - this is more evident on the ‘car’ category. Conversely, a bigger overlap of a relatively less distinguishable score range (0.4-0.6) can be improved by reweighing the scores. In this way, the probabilistic approach proposed in this work was applied to perform a ‘smoothing’ on the classification scores to mitigate overconfidence, as can be seen from Fig. 22 (Appendix A), regarding the pedestrian class. Overall, we can say that the results achieved by the *ML* and *MAP* layers for the car and cyclist categories showed quite similar results compared to the baseline. Such results can be seen in Table III, this implies that the approach may compromise slightly the overall performance. However, the proposed technique tends to perform better on the ‘hard’ level objects. We can conclude that, because the baseline implementation on SECOND does not attained overconfident behaviour, as shown by the results, the proposed approach degraded a bit the overall performance for that particular detector

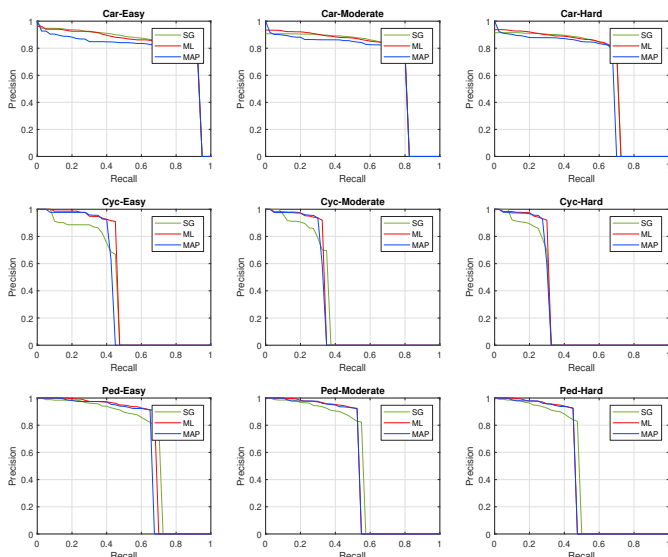


Fig. 14: Precision-recall curves using the RaV modality, with  $\lambda_{ML} = 5 \times 10^{-4}$ ,  $Bins_{ML} = 20$ ,  $\lambda_{MAP} = 1 \times 10^{-6}$ , and  $Bins_{MAP} = 24$ .

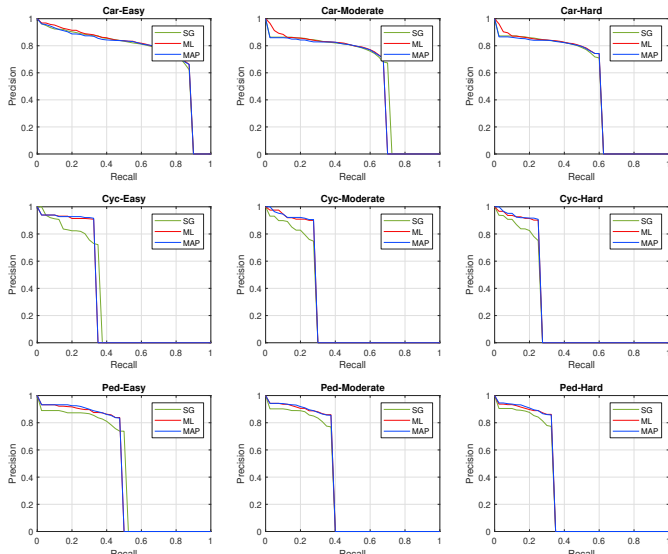


Fig. 15: Precision-recall curves for ReV modality, with  $\lambda_{ML} = 1 \times 10^{-4}$ ,  $Bins_{ML} = 23$ ,  $\lambda_{MAP} = 5 \times 10^{-5}$ , and  $Bins_{MAP} = 5$ .

but, on the other hand, it smoothed the scores for the false positives (which is very desirable in autonomous driving) having the advantage of giving probabilistic interpretation to the detectors.

## VI. CONCLUDING REMARKS

Many machine learning models, particularly deep learning ones, have the tendency of regarding the values of the detected objects' scores as being a degree of confidence (or related to a probability) *i.e.*, most models consider the scores as a degree of confidence of the obtained predictions. However, this is not completely true because, in most

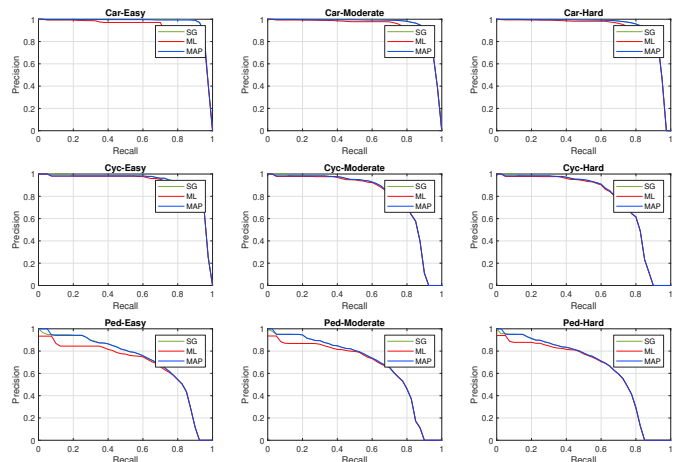


Fig. 16: Precision-recall curves using the RGB (camera) modality, with  $\lambda_{ML} = 5 \times 10^{-3}$ ,  $Bins_{ML} = 22$ ,  $\lambda_{MAP} = 1 \times 10^{-4}$ , and  $Bins_{MAP} = 24$ .

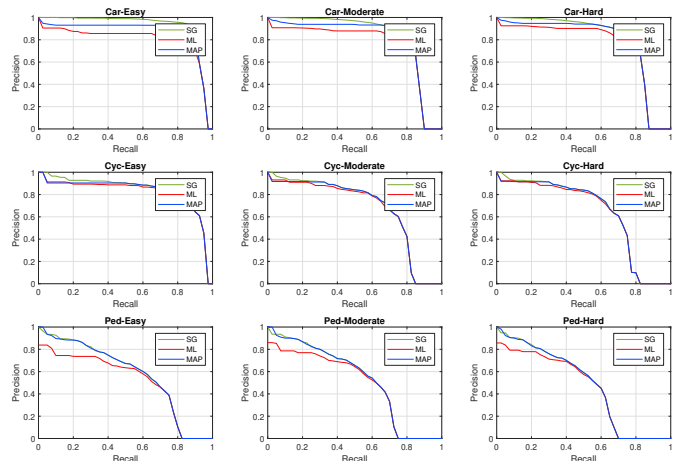


Fig. 17: Precision-recall using the SECOND on 3D point-clouds, with  $\lambda_{ML} = 5 \times 10^{-4}$ ,  $Bins_{ML} = 20$ ,  $\lambda_{MAP} = 1 \times 10^{-6}$ , and  $Bins_{MAP} = 24$ .

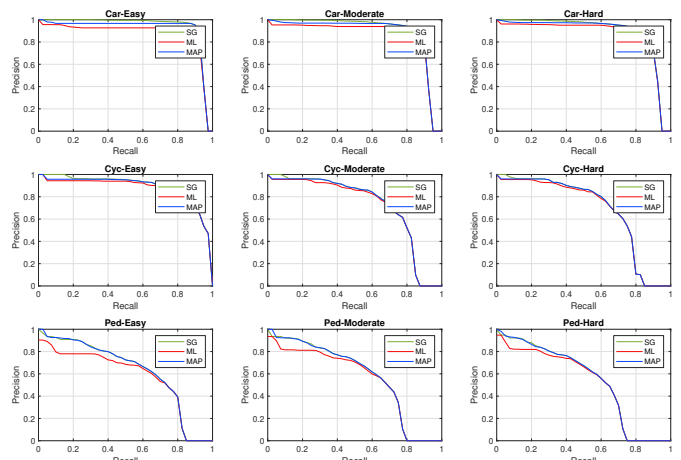


Fig. 18: Precision-recall curves considering BEV detection, with  $\lambda_{ML} = 1 \times 10^{-4}$ ,  $Bins_{ML} = 23$ ,  $\lambda_{MAP} = 5 \times 10^{-5}$ , and  $Bins_{MAP} = 5$ .

cases, the deep models are not generated through a regularized or a calibrated formalism that would allow a proper interpretation of confidence or uncertainty on the predictions. As a way to validate the claim that the scores of such detection cannot be interpreted as an actual probabilistic prediction, this work presented relevant results focused on out-of-distribution predicted objects motivated by critical situations, related to safety and decision-making, that may happen in real-world applications in autonomous driving.

To mitigate the gap between predicted scores from deep models and values that represent probabilistic predictions, many calibration and regularization techniques have been proposed by the scientific community - and it is still an open problem. However, the developments of such techniques are quite challenging, for instance because there is no ground truth available on uncertainty data for training.

The state-of-the-art formalism to capture model uncertainties (calibration and regularization techniques), during training or at the time test phase, aim to ensure confidence measures for the predictions of the models. In this way, this paper proposes a formulation (called ML/MAP layers) to reduce the overconfidence of detected false positive objects without degrading the classification scores of true positives *i.e.*, the ML/MAP layers are able to reduce confidence in incorrect predictions. The formulation takes into account a probabilistic inference through two models, one being non-parametric (normalized histogram) and the other is parametric (Gaussian density to model the priors for the MAP).

As a way to present the efficiency of the proposed probabilistic inference approach, this work considered different modalities, as RGB images, RaV, and ReV maps, as well as 3D point clouds data *i.e.*, datasets with different characteristics. In the case of RGB images, the characteristics are obtained directly from the camera, while RaV and ReV maps are obtained from depth (range-view) and intensity (reflectance-view) data, respectively.

The results achieved by the proposed approach are very satisfactory, specially for the minority category ‘cyclists’ (for YOLOV4), and ‘pedestrian’ case (for SECOND), as evidenced by the performance measures (Pr-Rc curves and AUC). Finally, a key advantage of the proposed approach is that there is no need to perform a new network training, that is, the approach has been applied in already trained networks.

## REFERENCES

- [1] J. Janai, F. Güney, A. Behl, and A. Geiger, “Computer vision for autonomous vehicles: Problems, datasets and state of the art,” *Foundations and Trends in Computer Graphics and Vision*, vol. 12, no. 1–3, pp. 1–308, 2020.
- [2] S. Liu, L. Li, J. Tang, S. Wu, and J.-L. Gaudiot, “Creating autonomous vehicle systems,” *Synthesis Lectures on Computer Science*, vol. 6, no. 1, pp. i–186, 2017.
- [3] L. Claussmann, M. Revilloud, D. Gruyer, and S. Glaser, “A review of motion planning for highway autonomous driving,” *IEEE Transactions on Intelligent Transportation Systems*, vol. 21, no. 5, pp. 1826–1848, 2020.
- [4] W. Maddern, G. Pascoe, C. Linegar, and P. Newman, “1 Year, 1000km: The Oxford RobotCar Dataset,” *The International Journal of Robotics Research*, vol. 36, no. 1, pp. 3–15, 2017.
- [5] S. Aly, “Partially occluded pedestrian classification using histogram of oriented gradients and local weighted linear kernel support vector machine,” *IET Computer Vision*, vol. 8, no. 6, pp. 620–628, 2014.
- [6] D. Su, H. Zhang, H. Chen, J. Yi, P.-Y. Chen, and Y. Gao, “Is robustness the cost of accuracy? A comprehensive study on the robustness of 18 deep image classification models,” in *European Conference on Computer Vision*, 2018.
- [7] A. Bochkovskiy, C. Wang, and H. M. Liao, “Yolov4: Optimal speed and accuracy of object detection,” *CoRR*, vol. abs/2004.10934, 2020.
- [8] E. Zhang and Y. Zhang, *F-Measure*. Boston, MA: Springer US, 2009, pp. 1147–1147.
- [9] C. Goutte and E. Gaussier, “A probabilistic interpretation of precision, recall and f-score, with implication for evaluation,” in *Proceedings of the 27th European Conference on Advances in Information Retrieval Research*, ser. ECIR’05. Berlin, Heidelberg: Springer-Verlag, 2005, p. 345–359.
- [10] Y. LeCun, B. Boser, J. S. Denker, D. Henderson, R. E. Howard, W. Hubbard, and L. D. Jackel, “Backpropagation applied to handwritten zip code recognition,” *Neural Computation*, vol. 1, no. 4, pp. 541–551, 1989.
- [11] A. Krizhevsky, I. Sutskever, and G. E. Hinton, “Imagenet classification with deep convolutional neural networks,” in *Advances in Neural Information Processing Systems*, vol. 25, 2012.
- [12] C. Szegedy, V. Vanhoucke, S. Ioffe, J. Shlens, and Z. Wojna, “Rethinking the inception architecture for computer vision,” in *IEEE Conference on Computer Vision and Pattern Recognition*, 2016, pp. 2818–2826.
- [13] M. Tan and Q. V. Le, “Efficientnet: Rethinking model scaling for convolutional neural networks,” in *PMLR Proceedings of the 36th International Conference on Machine Learning*, vol. 97, 2019, pp. 6105–6114.
- [14] A. Dosovitskiy, L. Beyer, A. Kolesnikov, D. Weissenborn, X. Zhai, T. Unterthiner, M. Dehghani, M. Minderer, G. Heigold, S. Gelly, J. Uszkoreit, and N. Houlsby, “An image is worth 16x16 words: Transformers for image recognition at scale,” in *9th International Conference on Learning Representations*, 2021.
- [15] I. O. Tolstikhin, N. Houlsby, A. Kolesnikov, L. Beyer, X. Zhai, T. Unterthiner, J. Yung, A. Steiner, D. Keysers, J. Uszkoreit, M. Lucic, and A. Dosovitskiy, “Mlp-mixer: An all-mlp architecture for vision,” *CoRR*, vol. abs/2105.01601, 2021.
- [16] R. McAllister, Y. Gal, A. Kendall, M. van der Wilk, A. Shah, R. Cipolla, and A. Weller, “Concrete problems for autonomous vehicle safety: Advantages of bayesian deep learning,” in *Proceedings of the Twenty-Sixth International Joint Conference on Artificial Intelligence*, 2017, pp. 4745–4753.
- [17] D. Feng, A. Harakeh, S. L. Waslander, and K. Dietmayer, “A review and comparative study on probabilistic object detection in autonomous driving,” *IEEE Transactions on Intelligent Transportation Systems*, pp. 1–20, 2021.
- [18] G. Melotti, C. Premebida, J. J. Bird, D. R. Faria, and N. Gonçalves, “Probabilistic object classification using CNN ML-MAP layers,” in *Workshop on Perception for Autonomous Driving, European Conference on Computer Vision*, 2020.
- [19] D. Feng, Z. Wang, Y. Zhou, L. Rosenbaum, F. Timm, K. Dietmayer, M. Tomizuka, and W. Zhan, “Labels are not perfect: Inferring spatial uncertainty in object detection,” *IEEE Transactions on Intelligent Transportation Systems*, pp. 1–14, 2021.
- [20] D. Feng, L. Rosenbaum, F. Timm, and K. Dietmayer, “Labels are not perfect: Improving probabilistic object detection via label uncertainty,” in *Workshop on Perception for Autonomous Driving, European Conference on Computer Vision*, 2020.
- [21] R. Krishnan and O. Tickoo, “Improving model calibration with accuracy versus uncertainty optimization,” in *Advances in Neural Information Processing Systems*, vol. 33, 2020, pp. 18 237–18 248.
- [22] D. P. P. Mesquita, L. A. Freitas, J. P. P. Gomes, and C. L. C. Mattos, “LS-SVR as a bayesian RBF network,” *IEEE Transactions on Neural Networks and Learning Systems*, pp. 1–5, 2019.
- [23] N. Passalis, M. Tzelepi, and A. Tefas, “Probabilistic knowledge transfer for lightweight deep representation learning,” *IEEE Transactions on Neural Networks and Learning Systems*, pp. 1–10, 2020.
- [24] K. Posch and J. Pilz, “Correlated parameters to accurately measure uncertainty in deep neural networks,” *IEEE Transactions*

- on *Neural Networks and Learning Systems*, vol. 32, no. 3, pp. 1037–1051, 2021.
- [25] D. Feng, L. Rosenbaum, F. Timm, and K. Dietmayer, “Leveraging heteroscedastic aleatoric uncertainties for robust real-time lidar 3D object detection,” in *IEEE Intelligent Vehicles Symposium*, 2019, pp. 1280–1287.
  - [26] Y. Zou, Z. Yu, X. Liu, B. V. K. V. Kumar, and J. Wang, “Confidence regularized self-training,” in *IEEE International Conference on Computer Vision*, 2019, pp. 5981–5990.
  - [27] C. Guo, G. Pleiss, Y. Sun, and K. Q. Weinberger, “On calibration of modern neural networks,” in *Proceedings of the 34th International Conference on Machine Learning*, vol. 70, 2017, pp. 1321–1330.
  - [28] G. Pereyra, G. Tucker, J. Chorowski, L. Kaiser, and G. E. Hinton, “Regularizing neural networks by penalizing confident output distributions,” ser. CoRR, arXiv: 1701.06548, 2017.
  - [29] Y. Gal and Z. Ghahramani, “Dropout as a bayesian approximation: Representing model uncertainty in deep learning,” in *PMLR Proceedings of The 33rd International Conference on Machine Learning*, vol. 48, 2016, pp. 1050–1059.
  - [30] D. P. Kingma, T. Salimans, and M. Welling, “Variational dropout and the local reparameterization trick,” in *Advances in Neural Information Processing Systems*, vol. 28. Curran Associates, Inc., 2015.
  - [31] C. Blundell, J. Cornebise, K. Kavukcuoglu, and D. Wierstra, “Weight uncertainty in neural network,” in *PMLR Proceedings of the 32nd International Conference on Machine Learning*, vol. 37, 2015, pp. 1613–1622.
  - [32] D. Kingma and M. Welling, “Auto-encoding variational Bayes,” in *ICLR Proceedings 2nd International Conference on Learning Representations*, 2014.
  - [33] A. Graves, “Practical variational inference for neural networks,” in *24th Advances in Neural Information Processing Systems*, vol. 24, 2011, pp. 2348–2356.
  - [34] A. Kristiadi, M. Hein, and P. Hennig, “Being bayesian, even just a bit, fixes overconfidence in relu networks,” *arXiv preprint arXiv:2002.10118*, 2020.
  - [35] S. Thulasidasan, G. Chennupati, J. A. Bilmes, T. Bhattacharya, and S. Michalak, “On mixup training: Improved calibration and predictive uncertainty for deep neural networks,” in *Advances in Neural Information Processing Systems 32*, 2019, pp. 13 888–13 899.
  - [36] K. B. Bulatov and D. V. Polevoy, “Reducing overconfidence in neural networks by dynamic variation of recognizer relevance,” in *Proceedings 29th European Conference on Modelling and Simulation*, 2015, pp. 488–491.
  - [37] Š. Raudys, R. Somorjai, and R. Baumgartner, “Reducing the overconfidence of base classifiers when combining their decisions,” in *Multiple Classifier Systems*, 2003, pp. 65–73.
  - [38] D. Feng, L. Rosenbaum, and K. Dietmayer, “Towards safe autonomous driving: Capture uncertainty in the deep neural network for lidar 3D vehicle detection,” in *IEEE 21st International Conference on Intelligent Transportation Systems*, 2018, pp. 3266–3273.
  - [39] Y. Wen, P. Vicol, J. Ba, D. Tran, and R. Grosse, “Flipout: Efficient pseudo-independent weight perturbations on mini-batches,” in *ICLR 6th International Conference on Learning Representations*, 2018.
  - [40] A. Kendall and Y. Gal, “What uncertainties do we need in bayesian deep learning for computer vision?” in *Advances in Neural Information Processing Systems 30*, 2017, pp. 5574–5584.
  - [41] B. Lakshminarayanan, A. Pritzel, and C. Blundell, “Simple and scalable predictive uncertainty estimation using deep ensembles,” in *Advances in Neural Information Processing Systems*, vol. 30, 2017, pp. 6402–6413.
  - [42] Y. Gal, J. Hron, and A. Kendall, “Concrete dropout,” in *31st Advances in Neural Information Processing Systems*, vol. 30, 2017.
  - [43] M. Lukasik, S. Bhojanapalli, A. Menon, and S. Kumar, “Does label smoothing mitigate label noise?” in *PMLR Proceedings of the 37th International Conference on Machine Learning*, vol. 119, 2020, pp. 6448–6458.
  - [44] L. Neumann, A. Zisserman, and A. Vedaldi, “Relaxed softmax: Efficient confidence auto-calibration for safe pedestrian detection,” in *NIPS Workshop on Machine Learning for Intelligent Transportation System*, 2018.
  - [45] C. Corbière, N. THOME, A. Bar-Hen, M. Cord, and P. Pérez, “Addressing failure prediction by learning model confidence,” in *Advances in Neural Information Processing Systems*, vol. 32, 2019.
  - [46] D. Hendrycks and K. Gimpel, “A baseline for detecting misclassified and out-of-distribution examples in neural networks,” in *5th International Conference on Learning Representations*, 2017.
  - [47] I. J. Goodfellow, J. Shlens, and C. Szegedy, “Explaining and harnessing adversarial examples,” *CoRR, arXiv*, vol. 1412.6572, 2015.
  - [48] C. Szegedy, W. Zaremba, I. Sutskever, J. Bruna, D. Erhan, I. Goodfellow, and R. Fergus, “Intriguing properties of neural networks,” in *International Conference on Learning Representations*, 2014.
  - [49] T. DeVries and G. W. Taylor, “Learning confidence for out-of-distribution detection in neural networks,” *CoRR, arXiv:1802.04865*, 2018.
  - [50] S. Liang, Y. Li, and R. Srikant, “Enhancing the reliability of out-of-distribution image detection in neural networks,” in *6th International Conference on Learning Representations*, 2018.
  - [51] Y. Gal, “Uncertainty in deep learning,” Ph.D. dissertation, University of Cambridge, 2016.
  - [52] C. M. Bishop, *Pattern Recognition and Machine Learning*. Springer, 2006.
  - [53] I. J. Goodfellow, Y. Bengio, and A. Courville, *Deep Learning*, ser. Adaptive Computation and Machine Learning. MIT Press, 2016.
  - [54] D. Molchanov, A. Ashukha, and D. Vetrov, “Variational dropout sparsifies deep neural networks,” in *PMLR Proceedings of the 34th International Conference on Machine Learning*, vol. 70, 2017, pp. 2498–2507.
  - [55] A. Papoulis and U. Pillai, *Probability, random variables and stochastic processes*, 4th ed. McGraw-Hill, Nov. 2001.
  - [56] D. Valcarce, J. Parapar, and Á. Barreiro, “Additive smoothing for relevance-based language modelling of recommender systems,” in *Proceedings of the 4th Spanish Conference on Information Retrieval*, 2016.
  - [57] S. F. Chen and J. Goodman, “An empirical study of smoothing techniques for language modeling,” Harvard Computer Science Group Technical Report, Tech. Rep., 1998.
  - [58] G. J. Lidstone, “Note on the general case of the bayes-laplace formula for inductive or a posteriori probabilities,” *Transactions of the Faculty of Actuaries*, vol. 8, p. 182–192, 1920.
  - [59] Z. Zheng, P. Wang, W. Liu, J. Li, R. Ye, and D. Ren, “Distance-iou loss: Faster and better learning for bounding box regression,” *Proceedings of the AAAI Conference on Artificial Intelligence*, vol. 34, no. 07, pp. 12 993–13 000, 2020.
  - [60] I. Loshchilov and F. Hutter, “SGDR: stochastic gradient descent with warm restarts,” in *5th International Conference on Learning Representations*, 2017.
  - [61] Z. Yao, Y. Cao, S. Zheng, G. Huang, and S. Lin, “Cross-iteration batch normalization,” in *IEEE Conference on Computer Vision and Pattern Recognition*, 2021.
  - [62] Y. Yan, Y. Mao, and B. Li, “Second: Sparsely embedded convolutional detection,” *Sensors*, vol. 18, no. 10, p. 3337, 2018.
  - [63] G. Melotti, C. Pretebida, and N. Gonçalves, “Multimodal deep-learning for object recognition combining camera and LIDAR data,” in *IEEE International Conference on Autonomous Robot Systems and Competitions*, 2020, pp. 177–182.

## APPENDIX A

### RESULTS OF THE PROPOSED APPROACH THROUGH HISTOGRAMS

The values of the output-scores from the proposed approach are summarized by histograms shown in the Figures 19, and 20 for the YOLOV4 detector, while Figures 21, 22 represent the histograms of the scores using the SECOND detector.

The baseline results achieved by YOLOV4 present many false positives (FP) with overconfidence scores, while the



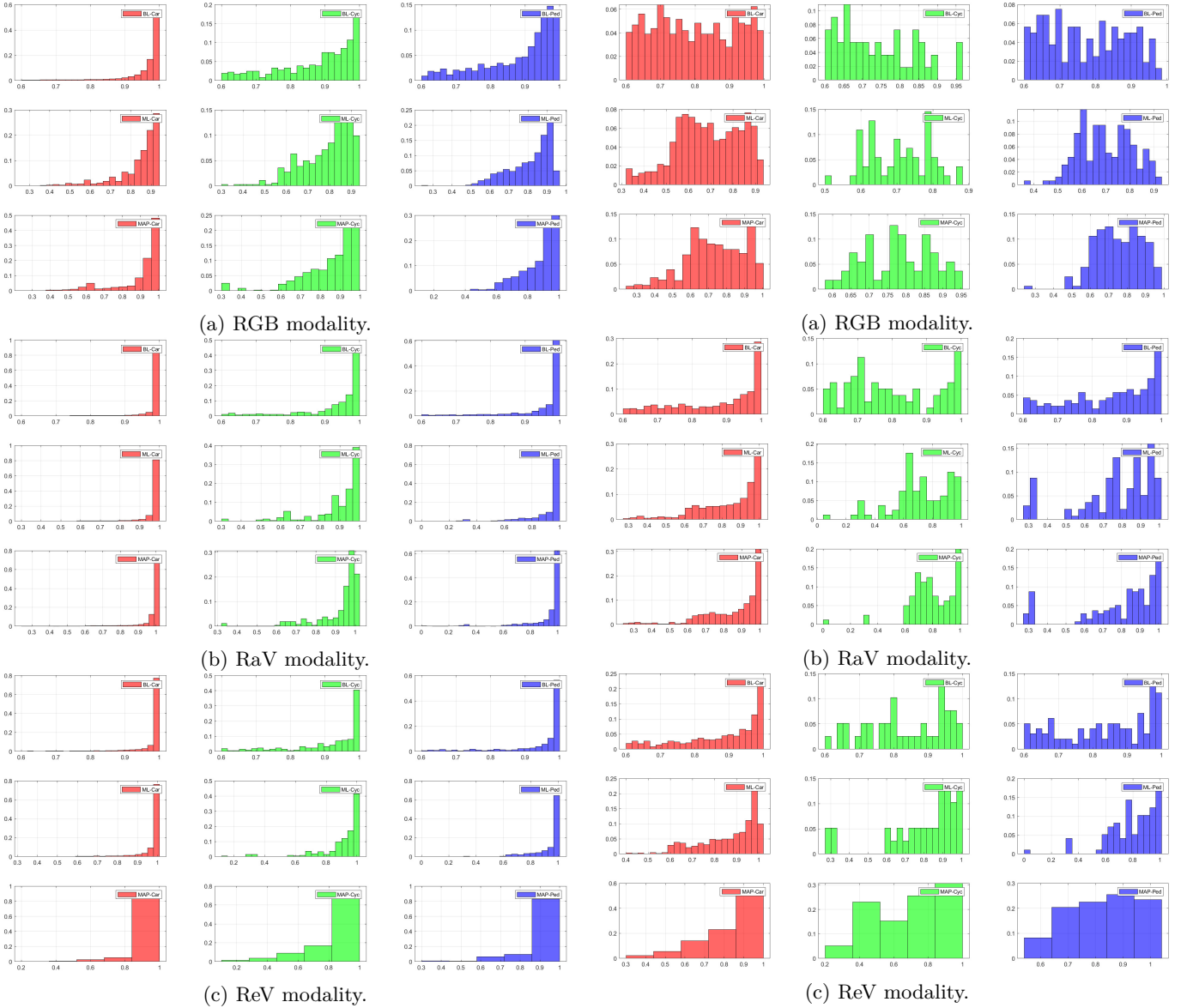


Fig. 19: Score distributions considering TP objects from YOLOV4 detector.

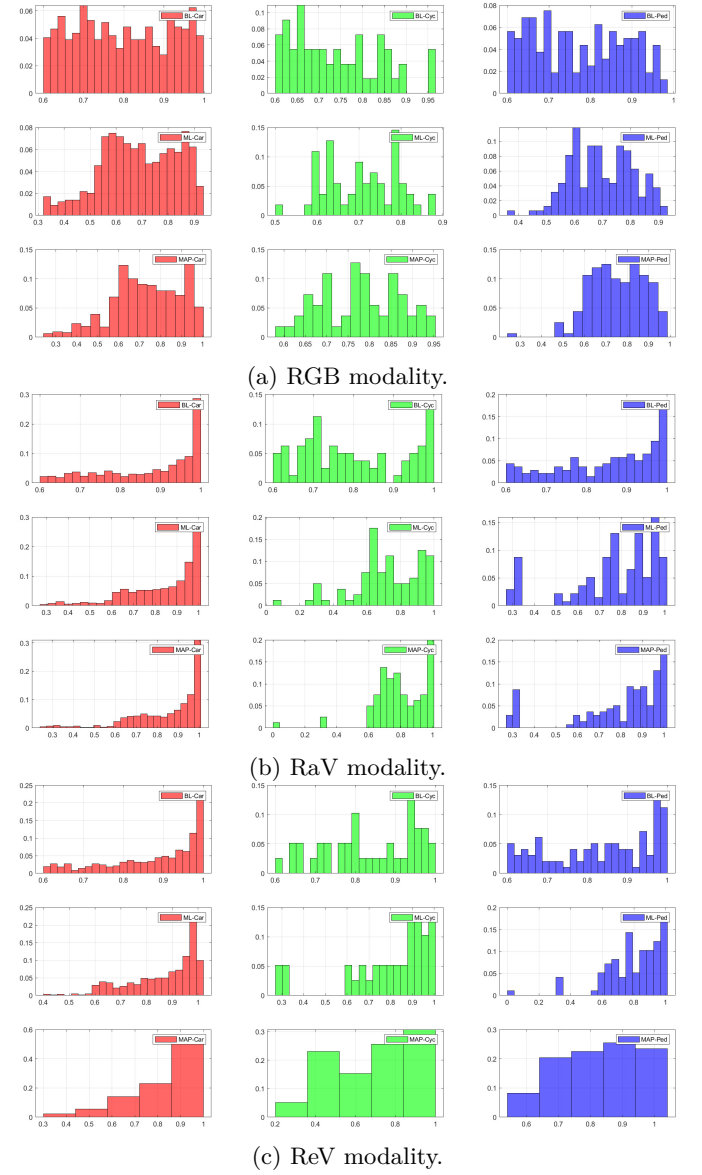


Fig. 20: Score distributions considering FP objects from YOLOV4 detector.

*ML* and *MAP* layers have shown very satisfactory results by reducing the overconfidence on the FPs, as well as did not harm the performance on the true positives (TP), according to the precision-recall curves (Figures 13, 14, and 15).

As the SECOND detector provides a relatively regularized scores across the classes, the *ML* and *MAP* approaches have limited improvement by eliminating the high-scoring FPs. However, the probabilistic approach is able to distinguish the ambiguous scores from the pedestrian class. This can be shown by the more overlap score range of true and false positive objects (Figures 16, 17, 18, 21, and 22).

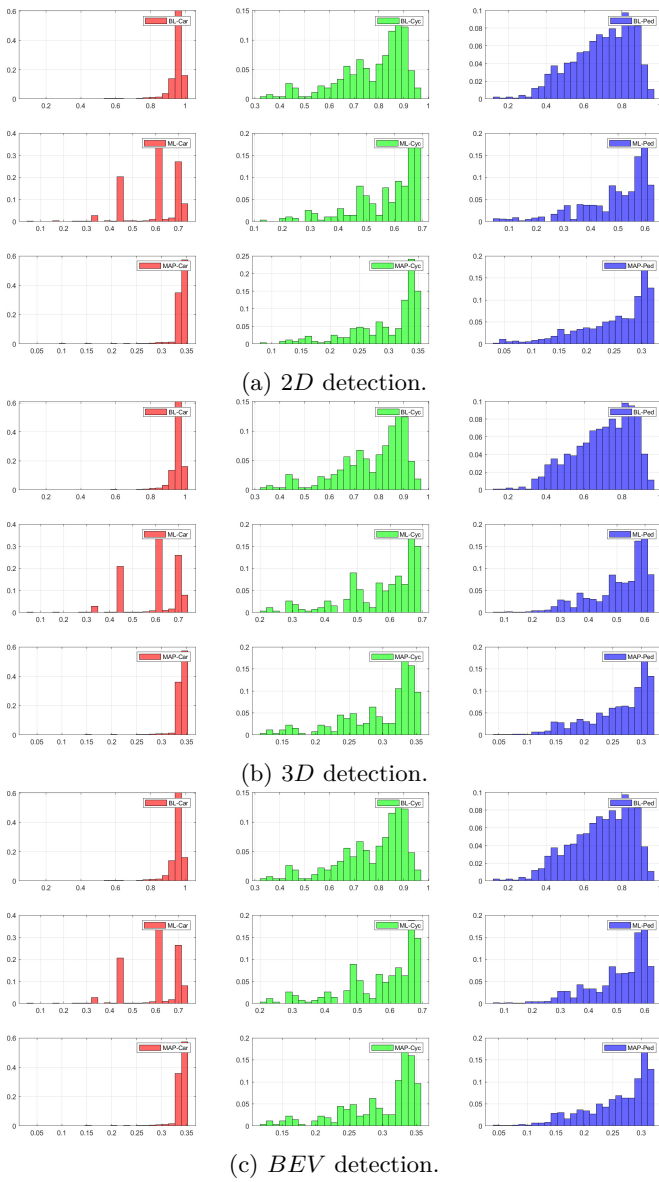


Fig. 21: Score distributions considering TP objects from SECOND detector.

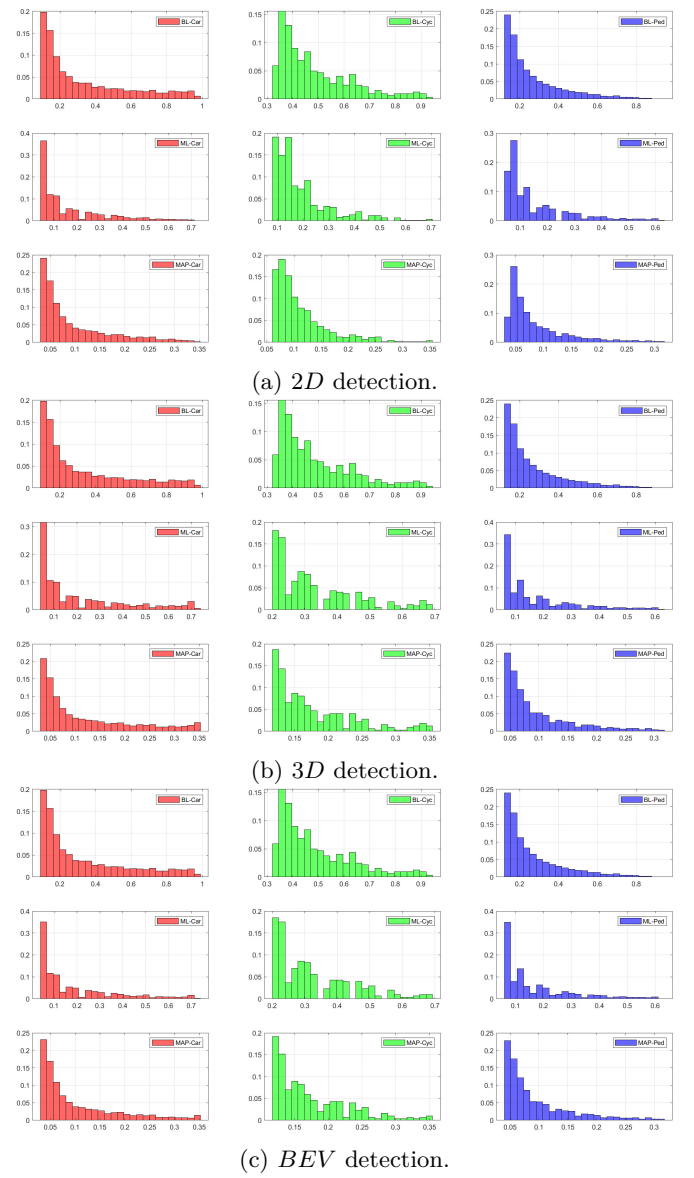


Fig. 22: Score distributions considering FP objects from SECOND detector.